BIOENG

Brazilian Journal of Biosystems Engineering (2024), 18 1219

REGULAR ARTICLE

Bean yield estimation using unmanned aerial vehicle imagery

Diane Gomes Campos[1], Rodrigo Nogueira Martins[1]

[1]Federal Institute of Northern Minas Gerais - IFNMG, Campus Araçuaí, MG, Brazil.

Regular Section
Academic Editor: Celso Antonio Goulart

Statements and Declarations

Data availability
All data will be shared if requested.

Institutional Review Board Statement
Not applicable

Conflicts of interest
The authors declare no conflict of interest.

Funding and Acknowledgements
We thank the Instituto Federal do Norte de Minas Gerais (IFNMG), Campus Araçuaí for supporting the researchers.

Autor contribution
DGC: Conceptualization, Experimental data collection, Data custody, Data analysis, Writing the manuscript; RNM: Supervision, Conceptualization, Experimental data collection, Data custody, Data analysis, Writing the manuscript, Manuscript Review.

Abstract

The common bean is a crop of substantial socioeconomic importance that is cultivated throughout the Brazilian territory. Despite that, studies conducted so far have shown limitations in the methodologies used for yield estimation. In this sense, emerging technologies such as unmanned aerial vehicles (UAVs) can help both in crop monitoring and in assessing crop yield. Therefore, this study aimed: (1) to estimate the bean yield using spectral variables derived from UAV imagery and (2) to define the best vegetative stage for yield estimation. For this, data from a field experiment were used. The beans were planted in a conventional system in an area of 600 m² (20 x 30 m). During the crop cycle, six flights were carried out using a UAV equipped with a five-band multispectral camera (Red, Green, Blue, Red Edge, and Near-infrared). After that, 10 spectral variables composed of the bands and five vegetation indices (VIs) were obtained. At the end of the season, the area was harvested, and the yield (kg ha^{-1}) was determined. Then, the data was submitted to correlation (r), and regression analysis. Overall, all developed models showed moderate performance, but in accordance with the literature, with R^2 and RMSE values ranging from 0.52 to 0.57 and from 252.79 to 208.84 kg ha^{-1}, respectively. Regarding the best vegetative stage for yield estimation, the selected models used data from the second flight (52 days after planting) at the beginning of pod formation and filling (between stages R7 and R8).

Keywords

Digital agriculture; UAV. Vegetation index; *Phaseolus vulgaris* L.

Introduction

Nowadays, there exists a growing concern regarding global food security and environmental conservation, underlined by the need to achieve a projected 70% increase in food production by 2050 to accommodate the expanding world population. The common bean (*Phaseolus vulgaris* L.), a crop of substantial socioeconomic importance, is ubiquitously cultivated throughout Brazil, catering to the needs of small, medium, and large-scale producers (Hiolanda et al., 2018; de Andrade et al., 2020). Within the Brazilian culinary context, it assumes a pivotal role as a primary staple, distinguished for its role as a low-fat energy source. According to the CONAB (Brazilian National Supply Company), the national production in the 2022 harvest reached an average of 3083.6 tons, with a productivity of 1095.0 kg ha^{-1}, covering an area of 2816.1 ha (CONAB, 2022).

Bean cultivation is practiced throughout all Brazilian regions, and due to its short growth cycle (60-70 days), it offers the advantage of being planted in three distinct periods throughout the year. In this case, the first crop is considered between August and December, the second crop between January and April, and the third crop between May and July (CONAB, 2021). The ability to produce three crops annually has been made possible by advancements in field technologies, such as seed genetic improvement, more precise fertilization, and the use of irrigation to supplement the crop's water demand.

Thus, given the growing demand for food and the urgent need to feed the burgeoning population, early yield estimations became crucial for food security and agricultural practices (Ramos et al., 2020; Zhao et al., 2020). Moreover, yield estimates are fundamental to driving governmental policies, and for market behavior. The entire process of sales and decision-making must rely on an accurate estimate of the expected yield. Traditionally, the crop yield is estimated by harvesting a few plants on the field, whose yield is then extrapolated to the entire production area (Lipovac et al., 2022; Ranjan et al., 2019). These evaluations are time-consuming, labor-intensive, and most importantly destructive (Araus and Cairns, 2014; Bellvert et al., 2014). Moreover, despite this, only a fraction of farmers succeed in fully harnessing the productive potential of the crop and precisely forecasting crop yield. This is chiefly attributed to management challenges like

* Corresponding author
E-mail address: rodrigo.nogueira@ifnmg.edu.br (R.N. Martins)

https://doi.org/10.18011/bioeng.2024.v18.1219
Received: 08 March 2024 / Accepted: 19 April 2024 / Available online: 06 June 2024

inadequate use of fertilizers and soil amendments, aggravated by climatic factors (Finger et al., 2019; Nowak, 2021).

As a solution, precision agriculture (PA) offers a diversity of tools that can improve yield estimates. PA is a management strategy that takes account of temporal and spatial variability to improve sustainability of agricultural production (ISPA, 2024). Among its different tools, remote sensing (RS) have gained huge attention in agricultural crop production management (Ranjan et al., 2019). RS has the potential of playing a determinant role as a spatial information source. Moreover, RS-based technologies provide low-cost, timely and accurate information on crop status and have been effectively used in yield estimates of several crops (Da Silva et al., 2020; Gao et al., 2018; Hassan et al., 2019; Rehman et al., 2019). Recently, with the advent of Unmanned Aerial Vehicles (UAV platforms and miniaturization of Red-Green-Blue - RGB, multispectral and hyperspectral sensors, remote monitoring of crops has intensified. This technology is primarily based on the use of sensors (cameras) onboard UAV platforms, which have the advantages of convenient operation, high flexibility, and strong adaptability to the spatiotemporal resolution needed (Ji et al., 2022).

Recent studies on the bean crop have focused on using spectral information derived from UAV imagery for water stress and yield assessment (Ranjan et al., 2019; Zhou et al., 2018), yield prediction with different irrigation depths and sowing periods (Lipovac et al., 2022), plant height and yield estimation (Ji et al., 2022), phenotyping of bean cultivars tolerant to drought and low nitrogen stress (Sankaran et al., 2018) plant height, leaf area index and chlorophyll content estimation (Quille-Mamani et al., 2022), and yield prediction of different bean cultivars (Saravia et al., 2023).

All these studies were based on the use of vegetation indices (VIs) to assess the spectral response of the vegetation. VIs are mathematical combinations of different wavelengths. Normally, the VIs are used to highlight plant intrinsic characteristics that are related to crop characteristics (e.g., greenness, vigor, nutritional status, and crop yield) (Baloloy et al., 2020). Given the close relationship between VIs and the plant characteristics such as yield, it can be used as input for the development of yield estimation models. The relationship between the crop yield and the VIs is explained by the fact that yield is a function of canopy characteristics, such as chlorophyll content, biomass, and canopy architecture, whose association was already evaluated previously (Baio et al., 2018; Zhao et al. 2007; Zhao et al., 2020).

For the bean crop, the studies mentioned above, specifically those related to yield assessment have used spectral variables (bands and VIs) to reach their purpose. However, none of them considered the association of multiple spectral variables to improve model performance nor did they define the best vegetative stage for yield estimation. Therefore, this study aimed: (1) to estimate the bean yield using spectral variables (bands and VIs) derived from UAV imagery and (2) to define the best vegetative stage for yield estimation.

Materials and methods

Study area

The field experiment was conducted from April 2019 to August 2019 in an area of 600 m² at the Universidade Federal de Viçosa, municipality of Viçosa, southeastern Brazil (20°45' S, 42°52' W, and 649 m above sea level) (Figure 1). The climate in the area, according to the Köppen-Geiger classification system, is classified as humid subtropical with dry winter and hot summer (CWA) (Alvares et al., 2013). The soil was a Yellow-red Oxisol with a clay loam texture composed of 40 % clay, 18 % silt, and 42 % sand (Soil Survey Staff, 2014).

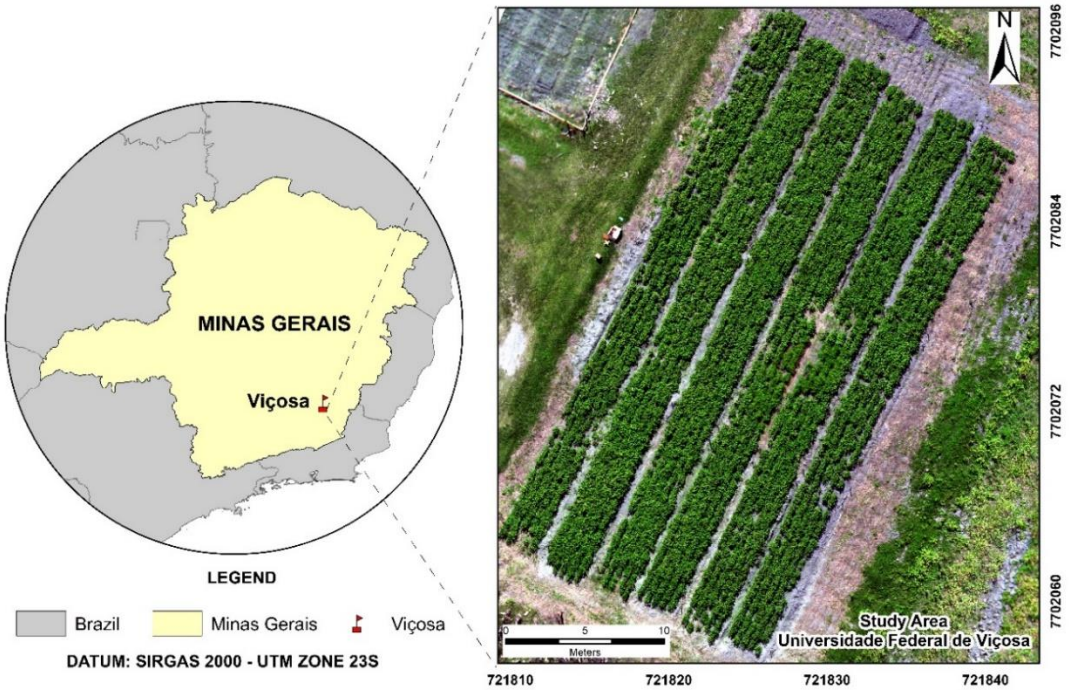

Figure 1. Location of the experimental field.

Crop traits

The crop used in the experiment was the common bean (*Phaseolus vulgaris* L.), variety Carioca. The bean was planted in a conventional system using an area that was divided into 18 experimental plots measuring 20 m² (2 x 10 m). Sowing was conducted on April 24th, 2019, with the application of 350 kg ha^{-1} of N-P_2O_5-K_2O (formulation: 4-14-8 %) distributed over the planting rows.

After planting, weed control was conducted using 2 L ha^{-1} of the herbicide Fusiflex. As for the slug control, 3 g m^{-2} of the insecticide Lesmax was applied. Lastly, the control of whiteflies and Diabrotica speciosa was conducted using 150 g ha^{-1} of the insecticide Evidence. The remaining crop traits were conducted following local procedures as described in Martins et al. (2021).

At the physiological maturity stage (September 8th, 2019), the bean plants from the three central rows within the useful area of each plot (useful area: 9 x 1 m) were manually harvested. Then, the bean moisture content was determined using the methodology established in the Seed Analysis Standards (Brasil, 2009). Finally, the bean yield (kg ha^{-1}) was adjusted to 13% moisture content

Data acquisition

Multispectral imagery acquisition and processing

Imagery acquisition in the study area was conducted using a multispectral camera MicaSense RedEdge MX (MicaSense, Seattle, WA, USA) onboard an unmanned aerial vehicle (UAV), DJI Matrice 100 (DJI Innovations, Shenzhen, China). The RedEdge MX is composed of five CMOS sensors (complementary metal oxide semiconductor) that capture the following bands: (1) blue (455–495 nm); (2) green (540–580 nm); (3) red (658–678 nm); (4) red edge (RE) (707–727 nm); and (5) near-infrared (NIR) (800–880 nm).

All UAV flights were conducted in autonomous mode with a flight plan previously defined in the laboratory using the DroneDeploy software (Infatics Inc. San Francisco, California, USA). In addition, the images from all flights were captured around 12:00h local time, aiming to minimize environmental effects, such as cloud presence and solar angle influence. The flights were carried out between June and July 2019 (Table 1) at 9.3 m s^{-1} speed with 80% and 75% of lateral and longitudinal overlap, respectively. Additionally, the flight altitude and spatial resolution of the orthomosaics were 25 m and 1.4 cm, respectively.

Table 1. Flight date, days after planting (DAP), and the vegetative stage

Flight date	DAP	Vegetative stage
07/06/2019	45	R5
14/06/2019	52	R7
24/06/2019	62	R7
05/07/2019	73	R8
23/07/2019	91	R8
31/07/2019	99	R9

R5: Pre-flowering; R7: Pod formation; R8: Pod filling; R9: Physiological maturity.

All UAV images were acquired with 12 bits in raw format, preserving the information (*e.g.*, contrast, sharpness, etc), without processing and compression at the time of acquisition. Next, to perform the radiometric calibration in postprocessing, before and after each flight, images of the reflectance calibration target provided by the MicaSense were taken at 1.00 m height. After that, the orthomosaics were obtained using the Agisoft™ MetaShape software, version 1.5.3 (Agisoft LLC, St. Petersburg, Russia) following the procedures from the image alignment to the creation, and georeferencing of the orthomosaics as detailed in Nogueira Martins et al. (2021). The orthomosaics were georeferenced in the QGIS software, version 3.2 (Team QGIS Development, 2016) using as reference 10 ground control points (GCP), previously placed in the experimental area. The GCPs were georeferenced using a GNSS (Global Navigation Satellite System), receiver Trimble ProXT (Trimble Inc., Sunnyvale, CA, USA).

Definition and extraction of the spectral variables

From the orthomosaics, the five spectral bands (RGB, Red Edge, and NIR) and the following VIs were obtained in the QGIS software: Normalized Difference Vegetation Index (NDVI); Green Normalized Difference Vegetation Index (GNDVI); Optimized Soil-Adjusted Vegetation Index (OSAVI); Normalized Difference Red Edge Index (NDRE); and Spectral Feature Depth Vegetation Index (SFDVI) (Table 2).

The use of VIs is crucial for minimizing the variability caused by external factors. VIs are sensitive to the plant biomass; hence, sensitive to the amount of chlorophyll present in a specific area. Coupled with that, the amount of biomass has been associated with the leaf area index and the crop yield in previous studies (Li et al., 2020; Macedo et al., 2023; da Silva et al., 2020; Yue et al., 2020). Based on that, the criteria for selecting the VIs were that: (1) the existing bands obtained by the multispectral camera could be used; and (2) that they had a good relationship with vegetation pigments and also with the crop nutritional status. Lastly, all spectral variables were obtained for the vegetative stages presented in Table 1.

To extract the spectral variables (VIs and spectral bands), polygon masks were delineated to cover the extension of the experimental plots using the QGIS software. Then, from the creation of the polygons, the average, minimum, maximum and standard deviation values of the reflectance of the spectral bands and VIs were extracted using the zonal statistics tool. Finally, a database was created in Excel using the extracted data for subsequent analysis.

Table 2. References and equations of the vegetation indices used in this study

Equation	Reference
NDVI = (N - R) / (N + R)	(Rouse et al., 1973)
GNDVI = (N - G) / (G + G)	(Gitelson et al., 1996)
OSAVI = (N - R) / (N + R + 0,16)	(Rondeaux et al., 1996)
SFDVI = ((N + G) / 2) - ((R + RE) / 2)	(Baptista, 2015)
NDRE = (N - RE) / (N + RE)	(Gitelson; Merzlyak, 1994)

R, Red; G, Green; B, Blue; N, Near-infrared; and RE, Red Edge band.

Data analysis

The spectral variables corresponding to different UAV flight dates, along with the bean yield data, were initially subjected to descriptive statistical analysis. This involved generating boxplots for all variables to provide a general characterization throughout the crop cycle. The normality of the data was assessed using the Shapiro-Wilk test. Next, a Pearson correlation analysis (r) was conducted to evaluate the degree of association between the spectral variables (spectral bands and VIs) and the crop yield. For this analysis, only correlations with values above 0.4 were selected to demonstrate the variables tending to exhibit a stronger association with the bean yield. The remaining results are available in supplementary material.

Subsequently, simple and multiple linear regression analyses were carried out considering the different UAV flight dates. The significance of the regression coefficients was assessed using the t-test at a 5% probability level ($p<0.05$). Then, to infer which spectral variable or the combination of variables between the different flight dates presented the best result for yield estimation, the following metrics were calculated: Coefficient of determination (R^2) and Root mean square error (RMSE). The selection of spectral variables to compose the regression models was carried out using the algorithm best subset regression through the 'olsrr' package (Hebbali, 2022). The algorithm fits all possible models using the spectral variables from all UAV flights and displays the best candidates based on the highest R^2 and lowest RMSE values. Lastly, all statistical analyses were performed using R software, version 3.6.3 (Team R Core, 2020).

Results and discussion

General characterization of the spectral variables and the bean yield

Boxplots of the temporal variation of the spectral variables on the six UAV flights carried out throughout the development of the bean crop are presented in Figure 2.

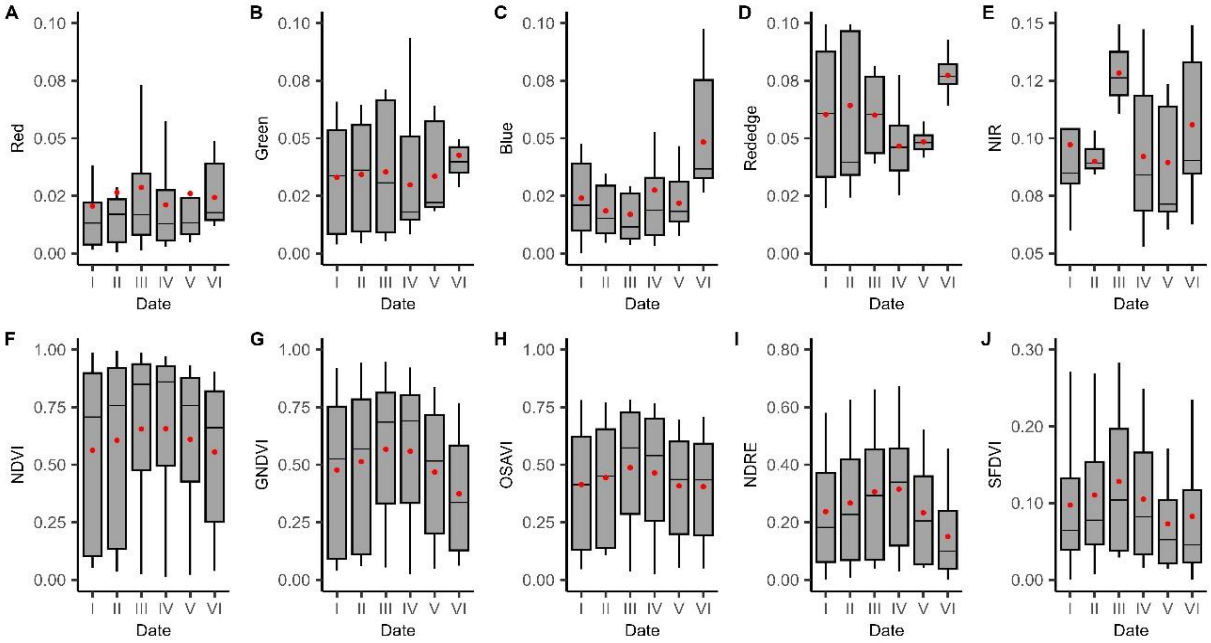

Figure 2. Boxplot of the temporal variation of the spectral bands (A, B, C, D and E) and vegetation indices (F, G, H, I and J).

As the plant develops to a certain point, under healthy conditions, it is expected that the spectral variables (VIs and bands) increase in accordance with their development up to the peak of vegetative vigor. This occurs due to the increase in the leaf area and, consequently, the plant canopy. This behavior was observed for all variables, except for the blue band (Figure 2C), up to the third flight carried out 62 days after planting (DAP). Then, for the remaining flights, a tendency of reduction in the spectral variables values was expected, as the crop began to reduce its vigor due to senescence, characterized

by changes in the leaf structure and a reduction in chlorophyll activity (Lipovac et al., 2022; Merzlyak et al., 2002; Martins et al., 2021). However, among the spectral variables (VIs and bands) used, only the VIs showed such behavior (Figure 2F to 2J).

This behavior may be related to the lack of radiometric normalization between the orthomosaics from different dates. In the spectral bands, this can result in variations in lighting conditions during image acquisition, which directly influences the reflectance values between different flight dates, even if the flights were carried out at the same time. On the other hand, although the VIs are also affected by this issue, the normalization between the bands used in their acquisition ends up reducing this effect (Mercante et al., 2009; Yuan; Elvidge, 1996).

Thus, considering the phenological development of the bean crop, only the VIs were able to represent the development of the plant in the field. Overall, the use of VIs, integrated into a certain period of crop development, or even the entire cycle, has been associated with agronomic parameters such as biomass, plant height, leaf area index, and crop yield (Prudente et al., 2019; Quille-Mamani et al., 2022; Saravia et al., 2023).

Regarding the crop yield variability, the values obtained from the experimental plots ranged from 2956.35 to 4459.56 kg ha^{-1}, with an average and standard deviation of 3709.85 and 427.89 kg ha^{-1}, respectively.

Correlation between the spectral variables and the crop yield

Results of the Pearson correlation (r) using the average, standard deviation, and minimum and maximum values of the spectral variables with bean yield are presented in Table 3. Similar to the average values, the other variables mentioned above were also extracted using the polygon masks in the experimental plots. These variables were used to identify variations in the crop's spectral response that, eventually, would not be identified when using only the average values.

Due to the number of variables and the number of flights performed, it was decided to present only the correlation values above 0.4. In this case, it was observed that the OSAVI and GNDVI indices, obtained using the maximum value, whose data was extracted from the second flight (52 DAP), tended to present the highest correlations with the crop yield ($r = 0.698$, $p < 0.01$; and $r = 0.573$, $p < 0.01$).

Compared to the metrics used, for the average data, the NDVI tended to show the greatest correlation ($r = 0.568$, $p < 0.01$), while for the standard deviation and minimum values, respectively, the SFDVI ($r = 0.530$, $p < 0.01$) and the blue band ($r = -0.546$, $p < 0.01$) stood out, with both being obtained at 52 DAP.

Lastly, the variables that tended to present correlations of greater magnitude with the crop yield, on a greater number of occasions throughout the UAV flights, were the NDVI, SFDVI, and OSAVI indices, and the NIR band. In general, this trend was observed in flights 1, 2, and 3. This can be explained by the fact that the plant entered the physiological maturity between the fourth (73 DAP) and fifth flight (91 DAP) (Procópio et al., 2009), which influenced its spectral response (Figure 2) and, consequently, the correlation results.

Table 3. Pearson correlation between the spectral variables and the crop yield using the average, standard deviation, and minimum and maximum values of these variables on different flight dates.

Average			Standard deviation		
Variable	Date	r	Variable	Date	r
NDVI	07/06	0.568***	SFDVI	07/06	0.481***
NDVI	24/06	0.491***	NDRE	07/06	0.471***
OSAVI	24/06	0.473***	RE	07/06	0.469***
RE	24/06	0.468***	NIR	07/06	0.490***
NIR	24/06	0.466***	SFDVI	14/06	0.530***
Minimum value			Maximum value		
BLUE	14/06	-0.546***	SFDVI	07/06	0.484***
GREEN	14/06	-0.466***	OSAVI	14/06	**0.698*** **
GNDVI	24/06	0.405**	GNDVI	14/06	**0.573*** **
NDVI	23/07	0.408*	NDRE	14/06	0.442***
NDRE	31/07	0.404**	NIR	24/06	0.403***

Bean yield estimation using spectral variables

After selecting the variables, the model obtained using the minimum values showed the best fit, *i.e.*, the highest R^2 and lowest RMSE (Figure 3C). Compared to the average yield obtained in the experimental plots (3709.85 kg ha^{-1}), the RMSE values obtained for the different regression models presented estimation errors that ranged from 5.63 to 6.81%. This is equivalent to an estimation error of 3 to 5 bags of beans in a total of 62 bags ha^{-1}.

Among the selected models, the variables that stood out most in their construction were the RED and NIR bands and the VI OSAVI (Table 4). Apart from the RED band, which showed no significant correlation ($p<0.05$) with the bean yield, the NIR band and the OSAVI index showed significant correlations on at least two flight dates, as discussed before (Table 3).

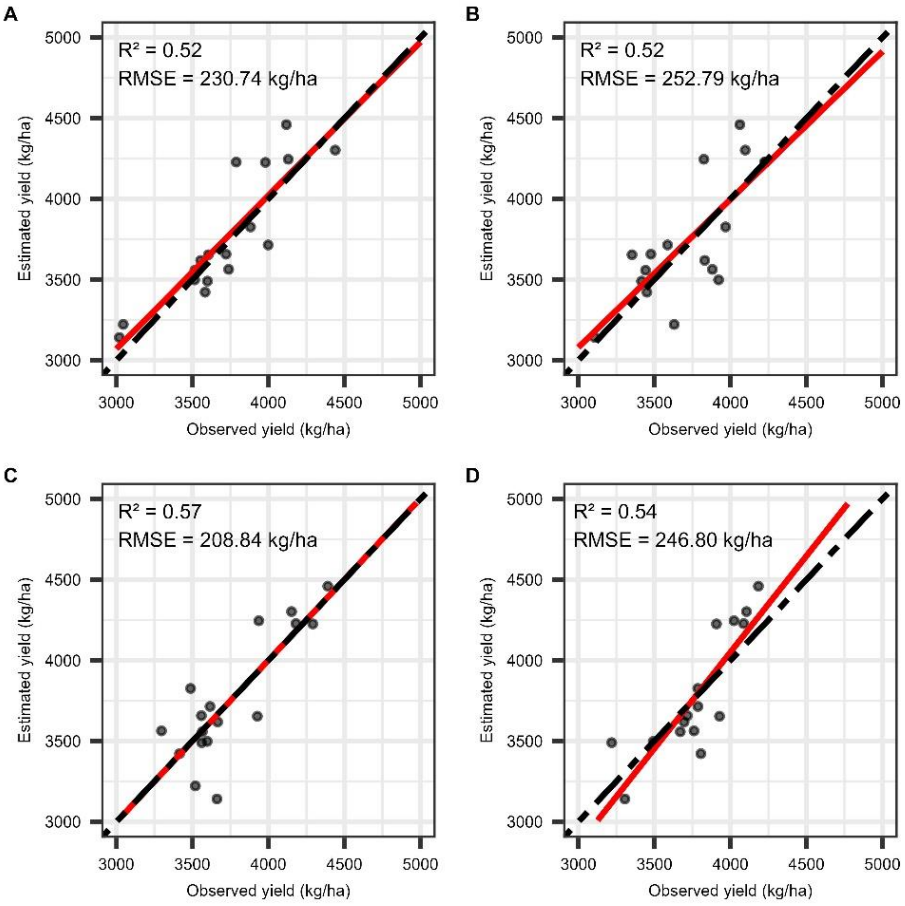

Figure 3. Scatterplots of the estimated versus observed values of the crop yield obtained using the average (A), standard deviation (B), minimum (C), and maximum values (D) of the spectral variables. Black and red lines refer to the proposed and the reference regression models (1:1).

Table 4. Best regression models for estimating the bean yield obtained using the average, standard deviation, minimum, and maximum values of the spectral variables on the six flight dates.

Average (Flight 6 – 99 DAP)
$Yield_{(kg/ha)}$ = - 133028.89 + 1019592.68 *RED* + 112529.85 *GREEN* – 42233.69 *BLUE* – 250615.29 *REDEDGE* + 209539.11 *NDVI* – 99608.35 *NDRE*
Standard deviation (Flight 3 – 74 DAP)
$Yield_{(kg/ha)}$ = 4438.197 + 253308.69 *REDEDGE* – 325762.98 *NIR* + 59029.10 *OSAVI* + 479091.07 *SFDVI*
Minimum value (Flight 4 – 91 DAP)
$Yield_{(kg/ha)}$ = 4716.57 – 170177.92 *RED* + 137105.20 *GREEN* – 20371.60 *NIR* + 5421.08 *NDVI* + 14513.96 *GNDVI* – 16084.35 *OSAVI* + 40226.38 *NDRE*
Maximum value (Flight 2 – 52 DAP)
$Yield_{(kg/ha)}$ = - 2413.83 + 8315.51 *RED* – 9529.38 *BLUE* + 3832.23 *NIR* + 33716.97 *OSAVI*

DAP, days after planting.

In general, all the yield estimation models performed in line with those observed in the literature. In a previous study, Lipovac et al. (2022) used different VIs such as NDVI, GNDVI, and MCARI1 (Modified Chlorophyll Absorption in Reflectance Index 1) to estimate the bean yield under different water deficit conditions. The R^2 values obtained by these authors ranged from 0.20 to 0.70. They also pointed out that the VIs NDVI (R^2 = 0.65) and MCARI1 (R^2 = 0.70) were capable of estimating the bean yield satisfactorily.

In another study, Ranjan et al. (2019) used NDVI and GNDVI to estimate bean yield and reported R^2 values of 0.62 and 0.54, respectively. In turn, Ji et al. (2022) used the plant height extracted from UAV images to estimate the bean yield. These authors reported R^2 values ranging from 0.50 to 0.64

and RMSE values from 990.01 to 838.61 kg ha^{-1}. Finally, Zhou et al. (2018) observed correlations (r) ranging from 0.71 to 0.72 of the GNDVI and canopy cover with bean yield at 54 DAP in two crop cycles.

More recently, Saravia et al. (2023) predicted the bean yield of four cultivars using 11 VIs derived from UAV imagery. First, these authors evaluated the correlation between the VIs and the crop yield on 13 dates (From 33 DAP to 118 DAP) and reported significant associations with values varying from 0.28 to 0.63. As for the prediction models, the authors used a combination of models composed of three, four, and five VIs, and also a combination of the different VIs and flight dates through a principal component analysis. When considering the prediction of the four cultivars together, the R^2 values varied from 0.47 to 0.48. On the other hand, when the prediction was carried out individually for each cultivar, the results improved and ranged from 0,62 to 0.94. Although these results are more accurate than those observed in the present study, this reinforces the utility of UAV imagery to estimate or predict the bean yield before the harvest.

Regarding the best flight date for estimating the bean yield, there was no consensus between the selected models. However, in the four models, all dates were always from or after the second flight (52 DAP) at the beginning of the R7 vegetative stage. This finding is in line with the results observed by Saravia et al. (2023), who reported better prediction accuracies between the phenological stages R6 to R8. At these stages, the crop begins to form and fill the pods, which may have contributed to the better performance of the estimation models from this date onwards. Lastly, about the best variables, it was observed that the RED and NIR bands and the OSAVI index were present in most of the best yield estimation models.

Limitations and recommendations for future studies

The use of aerial remote sensing has expanded in monitoring different crops. For the bean crop, most studies using UAV images have been oriented toward monitoring diverse characteristics beyond productivity. Recent examples encompass plant height estimation (Ji et al., 2022; Quille-Mamani et al., 2022), water stress detection (Ranjan et al., 2019; Zhou et al., 2018), and the phenotyping of varieties resistant to drought and low doses of nitrogen (Sankaran et al., 2022).

Thus, a limitation exists in studies about yield estimation, hindering more intricate discussions regarding the performance of regression models developed utilizing spectral variables. This limitation further extends to the evaluation of the actual contribution of these variables to bean yield. Additionally, the paucity of studies correlating spectral variables with the yield data often involves the incorporation of other biometric variables into the estimation models, as previously elucidated in the discussion. Furthermore, apart from the constraint on the number of studies investigating bean yield estimation, there is still a need for the repetition of cycles (harvests) and more frequent monitoring to acquire a greater volume of data, as well as the use of more robust statistical models to improve analysis.

Conclusions

This study evaluated the potential of using UAV images for bean yield estimation. Additionally, efforts were made to identify the optimal timing and the most influential spectral variables for estimating the crop yield. Overall, all developed models demonstrated moderate performance (R^2 ranging from 0.52 to 0.57; and RMSE ranging from 252.79 to 208.84 kg ha^{-1}), aligning with findings observed in the existing literature.

Regarding the best date for estimating the bean yield, there was no consensus between the selected models. However, in the models developed, all dates were always from or after the second flight (52 DAP) at the beginning of pod formation and filling (between stages R7 and R8). Lastly, in terms of the most influential variables, it was observed that the Red (RED) and Near-Infrared (NIR) bands, along with the Optimized Soil-Adjusted Vegetation Index (OSAVI), were prevalent in the majority of the top-performing models. Additionally, the NIR band and the OSAVI index were among the variables that tended to exhibit correlations of greater magnitude with the crop yield, in a greater number of times throughout the flights carried out.

References

Alvares, C. A., Stape, J. L., Sentelhas, P. C., Gonçalves, J. D. M., & Sparovek, G. (2013). Köppen's climate classification map for Brazil. *Meteorologische zeitschrift*, *22*(6), 711-728. https://doi.org/10.1127/0941-2948/2013/0507.

Araus, J. L., & Cairns, J. E. (2014). Field high-throughput phenotyping: the new crop breeding frontier. *Trends in plant science*, *19*(1), 52-61. https://doi.org/10.1016/j.tplants.2013.09.008.

Baio, F. H. R., Neves, D. C., Campos, C. D. S., & Teodoro, P. E. (2018). Relationship between cotton productivity and variability of NDVI obtained by Landsat images. *Bioscience Journal*, *34*(Supplement 1), 197-205. https://doi.org/10.14393/BJ-v34n6a2018-39583.

Baloloy, A. B., Blanco, A. C., Ana, R. R. C. S., & Nadaoka, K. (2020). Development and application of a new mangrove vegetation index (MVI) for rapid and accurate mangrove mapping. *ISPRS Journal of Photogrammetry and Remote Sensing*, *166*, 95-117. https://doi.org/10.1016/j.isprsjprs.2020.06.001.

Baptista, G. D. M. (2015). Aplicação do Índice de Vegetação por Profundidade de Feição Espectral (SFDVI–Spectral Feature Depth Vegetation Index) em dados RapidEye.(Application of Spectral Feature Depth Vegetation Index (SFDVI) to RapidEye data). *Anais XVII Simpósio Brasileiro de Sensoriamento Remoto-SBSR, João Pessoa-PB, Brasil*, *25*.

Bellvert, J., Zarco-Tejada, P. J., Girona, J., & Fereres, E. J. P. A. (2014). Mapping crop water stress index in a 'Pinot-noir'vineyard: comparing ground measurements with thermal remote sensing imagery from an unmanned aerial vehicle. *Precision agriculture*, *15*, 361-376. https://doi.org/10.1007/s11119-013-9334-5.

Brasil, M. da A. P. e A. (2009). Regras para Análise de Sementes (1st ed.). https://www.gov.br/agricultura/pt-br/assuntos/insumos-agropecuarios/arquivos-publicacoes-insumos/2946_regras_analise__sementes.pdf

CONAB, C. N. de A. (2021). Acompanhamento da safra brasileira: grãos. Safra 2020/21. Décimo segundo levantamento, Junho 2022. Monitoramento Agricola - Safra 2020. https://www.conab.gov.br/info-agro/safras/graos/boletim-da-safra-de-graos.

CONAB, C. N. de A. (2022). Acompanhamento da safra brasileira: grãos. Safra 2021/22. Nono levantamento, Julho 2022. Monitoramento Agricola - Safra 2022. https://www.conab.gov.br/info-agro/safras/graos/boletim-da-safra-de-graos.

Da Silva, E. E., Baio, F. H. R., Teodoro, L. P. R., da Silva Junior, C. A., Borges, R. S., & Teodoro, P. E. (2020). UAV-multispectral and vegetation indices in soybean grain yield prediction based on in situ observation. *Remote Sensing Applications: Society and Environment*, *18*, 100318. https://doi.org/10.1016/j.rsase.2020.100318.

De Andrade, E. K. V., Rodrigues, R., Bard, G. D. C. V., da Silva Pereira, L., Baptista, K. E. V., Cavalcanti, T. F. M., ... & Gomes, V. M. (2020). Identification, biochemical characterization and biological role of defense proteins from common bean genotypes seeds in response to Callosobruchus maculatus infestation. *Journal of stored products research*, *87*, 101580. https://doi.org/10.1016/j.jspr.2020.101580.

Finger, R., Swinton, S. M., El Benni, N., & Walter, A. (2019). Precision farming at the nexus of agricultural production and the environment. *Annual Review of Resource Economics*, *11*, 313-335. https://doi.org/10.1146/annurev-resource-100518-093929.

Gao, F., Anderson, M., Daughtry, C., Karnieli, A., Hively, D., & Kustas, W. (2020). A within-season approach for detecting early growth stages in corn and soybean using high temporal and spatial resolution imagery. *Remote Sensing of Environment*, *242*, 111752. https://doi.org/10.1016/j.rse.2020.111752.

Gitelson, A. A., Kaufman, Y. J., & Merzlyak, M. N. (1996). Use of a green channel in remote sensing of global vegetation from EOS-MODIS. *Remote sensing of Environment*, *58*(3), 289-298. https://doi.org/10.1016/S0034-4257(96)00072-7.

Gitelson, A., & Merzlyak, M. N. (1994). Spectral reflectance changes associated with autumn senescence of Aesculus hippocastanum L. and Acer platanoides L. leaves. Spectral features and relation to chlorophyll estimation. *Journal of plant physiology*, *143*(3), 286-292. https://doi.org/10.1016/S0176-1617(11)81633-0.

Hassan, M. A., Yang, M., Rasheed, A., Yang, G., Reynolds, M., Xia, X., ... & He, Z. (2019). A rapid monitoring of NDVI across the wheat growth cycle for grain yield prediction using a multi-spectral UAV platform. *Plant science*, *282*, 95-103. https://doi.org/10.1016/j.plantsci.2018.10.022.

Hebbali, A., & Hebbali, M. A. (2017). Package 'olsrr'. Version 0.5, 3. https://cloud.r-project.org/web/packages/olsrr/olsrr.pdf.

Hiolanda, R., Machado, D. H., Candido, W. J., de Faria, L. C., & Dalchiavon, F. C. (2018). Desempenho de genótipos de feijão carioca no Cerrado Central do Brasil. *Revista de ciências agrárias*, *41*(3), 815-824. https://doi.org/10.19084/RCA17285.

ISPA. (2024). Precision Ag Definition. International Society of Precision Agriculture. https://www.ispag.org/about/definition.

Ji, Y., Chen, Z., Cheng, Q., Liu, R., Li, M., Yan, X., ... & Yang, T. (2022). Estimation of plant height and yield based on UAV imagery in faba bean (Vicia faba L.). *Plant Methods*, *18*(1), 26. https://doi.org/10.1186/s13007-022-00861-7.

Jw, R. (1973). Monitoring vegetation systems in the great plains with ERTS. In *Third NASA Earth Resources Technology Satellite Symposium, 1973* (Vol. 1, pp. 309-317).

Li, B., Xu, X., Zhang, L., Han, J., Bian, C., Li, G., ... & Jin, L. (2020). Above-ground biomass estimation and yield prediction in potato by using UAV-based RGB and hyperspectral imaging. *ISPRS Journal of Photogrammetry and Remote Sensing*, *162*, 161-172. https://doi.org/10.1016/j.isprsjprs.2020.02.013.

Lipovac, A., Bezdan, A., Moravčević, D., Djurović, N., Ćosić, M., Benka, P., & Stričević, R. (2022). Correlation between Ground Measurements and UAV Sensed Vegetation Indices for Yield Prediction of Common Bean Grown under Different Irrigation Treatments and Sowing Periods. *Water*, *14*(22), 3786. https://doi.org/10.3390/w14223786.

Macedo, F. L., Nóbrega, H., de Freitas, J. G., Ragonezi, C., Pinto, L., Rosa, J., & Pinheiro de Carvalho, M. A. (2023). Estimation of productivity and above-ground biomass for corn (Zea mays) via vegetation indices in Madeira Island. *Agriculture*, *13*(6), 1115. https://doi.org/10.3390/agriculture13061115.

Martins, R. N., Portes, M. F., e Moraes, H. M. F., Junior, M. R. F., Rosas, J. T. F., & Junior, W. D. A. O. (2021). Influence of tillage systems on soil physical properties, spectral response and yield of the bean crop. *Remote Sensing Applications: Society and Environment*, *22*, 100517. https://doi.org/10.1016/j.rsase.2021.100517.

Mercante, E., Lamparelli, R. A., Uribe-Opazo, M. A., & Rocha, J. V. (2009). Características espectrais da soja ao longo do ciclo vegetativo com imagens landsat 5/TM em área agrícola no oeste do Paraná. *Engenharia Agrícola*, *29*, 328-338. https://doi.org/10.1590/S0100-69162009000200016.

Merzlyak, M. N. et. al. Does a leaf absorb radiation in the near infrared (780-900 nm) region? A new approach to quantifying optical reflection, absorption and transmission of leaves. Photosynthesis Research, v. 72, 2002. https://doi.org/10.1023/A:1019823303951.

Nogueira Martins, R., de Carvalho Pinto, F. D. A., Marçal de Queiroz, D., Magalhães Valente, D. S., & Fim Rosas, J. T. (2021). A novel vegetation index for coffee ripeness monitoring using aerial imagery. *Remote Sensing*, *13*(2), 263. https://doi.org/10.3390/rs13020263.

Nowak, B. (2021). Precision agriculture: Where do we stand? A review of the adoption of precision agriculture technologies on field crops farms in developed countries. *Agricultural Research*, *10*(4), 515-522. https://doi.org/10.1007/s40003-021-00539-x.

Prudente, V. H. R., Mercante, E., Johann, J. A., Souza, C. H. W. D., Cattani, C. E. V., Mendes, I. S., & Caon, I. L. (2021). Use of terrestrial remote sensing to estimate soybeans and beans biophysical parameters. *Geocarto International*, *36*(7), 773-790. https://doi.org/10.1080/10106049.2019.1624982.

Quille-Mamani, J., Porras-Jorge, R., Saravia-Navarro, D., Valqui-Valqui, L., Herrera, J., Chávez-Galarza, J., & Arbizu, C. I. (2022). Assessment of vegetation indices derived from UAV images for predicting biometric variables in bean during ripening stage. *Idesia*, *40*(2), 39-45. http://dx.doi.org/10.4067/S0718-34292022000200039.

Ramos, A. P. M., Osco, L. P., Furuya, D. E. G., Gonçalves, W. N., Santana, D. C., Teodoro, L. P. R., ... & Pistori, H. (2020). A random forest ranking approach to predict yield in maize with uav-based vegetation spectral indices. *Computers and Electronics in Agriculture*, *178*, 105791. https://doi.org/10.1016/j.compag.2020.105791.

Ranjan, R., Chandel, A. K., Khot, L. R., Bahlol, H. Y., Zhou, J., Boydston, R. A., & Miklas, P. N. (2019). Irrigated pinto bean crop stress and yield assessment using ground based low altitude remote sensing technology. *Information Processing in Agriculture*, *6*(4), 502-514. https://doi.org/10.1016/j.inpa.2019.01.005.

Rehman, T. H., Borja Reis, A. F., Akbar, N., & Linquist, B. A. (2019). Use of normalized difference vegetation index to assess N status and predict grain yield in rice. *Agronomy Journal*, *111*(6), 2889-2898. https://doi.org/10.2134/agronj2019.03.0217.

Rondeaux, G., Steven, M., & Baret, F. (1996). Optimization of soil-adjusted vegetation indices. *Remote sensing of environment*, *55*(2), 95-107. https://doi.org/10.1016/0034-4257(95)00186-7.

Sankaran, S., Zhou, J., Khot, L. R., Trapp, J. J., Mndolwa, E., & Miklas, P. N. (2018). High-throughput field phenotyping in dry bean using small unmanned aerial vehicle based multispectral imagery. *Computers and Electronics in Agriculture*, *151*, 84-92. https://doi.org/10.1016/j.compag.2018.05.034.

Saravia, D., Valqui-Valqui, L., Salazar, W., Quille-Mamani, J., Barboza, E., Porras-Jorge, R., ... & Arbizu, C. I. (2023). Yield prediction of four bean (*Phaseolus vulgaris*) cultivars using vegetation indices based on multispectral images from UAV in an arid zone of Peru. *Drones*, *7*(5), 325. https://doi.org/10.3390/drones7050325.

Soil Survey Staff. Keys to soil taxonomy by soil survey staff. United States. Department of Agriculture Natural Resources Conservation Service. 12º ed, 2014.

Team, Q. D. (2016). QGIS geographic information system. *Open source geospatial foundation project*.

Team, R. C. (2020). R: A language and environment for statistical computing. R Foundation for Statistical Computing.

Yuan, D., & Elvidge, C. D. (1996). Comparison of relative radiometric normalization techniques. *ISPRS Journal of Photogrammetry and Remote Sensing*, *51*(3), 117-126. https://doi.org/10.1016/0924-2716(96)00018-4.

Yue, J., Feng, H., Li, Z., Zhou, C., & Xu, K. (2021). Mapping winter-wheat biomass and grain yield based on a crop model and UAV remote sensing. *International Journal of Remote Sensing*, *42*(5), 1577-1601. https://doi.org/10.1080/01431161.2020.1823033.

Zhao, D., Reddy, K. R., Kakani, V. G., Read, J. J., & Koti, S. (2007). Canopy reflectance in cotton for growth assessment and lint yield prediction. *European Journal of Agronomy*, *26*(3), 335-344. https://doi.org/10.1016/j.eja.2006.12.001.

Zhao, Y., Potgieter, A. B., Zhang, M., Wu, B., & Hammer, G. L. (2020). Predicting wheat yield at the field scale by combining high-resolution Sentinel-2 satellite imagery and crop modelling. *Remote Sensing*, *12*(6), 1024. https://doi.org/10.3390/rs12061024.

Zhou, J., Khot, L. R., Boydston, R. A., Miklas, P. N., & Porter, L. (2018). Low altitude remote sensing technologies for crop stress monitoring: A case study on spatial and temporal monitoring of irrigated pinto bean. *Precision agriculture*, *19*, 555-569.https://doi.org/10.1007/s11119-017-9539-0.